

Ultra-Short Peptide Grafting on Mesoporous Films and Its Impact on Ionic Mesopore Accessibility

Mohadeseh Bagherabadi^a, and Annette Andrieu-Brunsen ^{a*}

a. Department of Chemistry, Technical University of Darmstadt, Peter-Grünberg-Str. 4, 64287

Darmstadt, Germany.

* annette.andrieu-brunsen@tu-darmstadt.de

Abstract

An approach for direct in-pore solid-phase ultra-short peptide synthesis on mesoporous films using the amino acids arginine, leucine, and glycine is presented. Although the bound number of amino acids remains low, ionic mesopore accessibility can be gradually adjusted. The addition of arginine in up to five reaction cycles leads to a progressive increase in positive mesopore charge density which gradually increases anionic mesopore accessibility at acidic pH. At basic pH, the remaining silanol groups at the pore wall still dominate counter-charged cation mesopore accessibility. Thus, specific peptide sequence design is demonstrated to be a very sensitive tool for molecular transport control in nanoscale pores. Overall, the direct in-pore solid-phase ultra-short peptide synthesis on mesoporous films using the sequences of different amino acids opens up exciting opportunities for the development of innovative

materials with precisely tailored properties and functions based on specific peptide sequence design.

Keywords: short peptide; ion transport; solid-phase peptide synthesis; biofunctionalization; BODIPY; mesoporous silica, nanopores.

INTRODUCTION

Porous silica provides a large specific surface area and controlled nanoscale pore structures. By integrating peptides into porous silica, the resulting hybrid materials, so-called peptide-nanomaterial conjugates, become interesting for the loading and release of therapeutic agents in drug delivery systems ^{1, 2}, healthcare, and environmental monitoring ^{3, 4}. Surface peptide functionalization thereby imparts specific material properties, such as antimicrobial activities, antifouling characteristics, and enhanced biocompatibility ^{5, 6}. Various methods enable the conjugation of peptides to nanomaterials. These methods can be broadly categorized into covalent bonding ⁷, non-covalent interactions ⁸, self-assembly ⁹, and bioorthogonal chemistry ¹⁰. Among these methods, covalent bonding ensures stable conjugation, minimizing the probability of detachment or degradation of the peptide from the nanomaterial. This method has been broadly used for fabricating peptide-nanomaterial conjugates ¹¹⁻¹⁹. With respect to peptide functionalization of nanoscale pores, Ashkenasy et al. designed peptides for the detection of paraoxon as a small molecule ²⁰. They identified the most effective peptide receptor sequence for exceptionally efficient paraoxon detection by monitoring ion currents passing through nanopores functionalized with these peptides ²⁰. Furthermore, Tsutsui et al. demonstrated that the surface of Au micropores was modified with a synthetic peptide designed from toll-like receptor 5 (TLR5), which exhibited intermolecular interactions with *Escherichia coli* ²¹. Brodrecht et al. ²² have recently conducted direct solid-phase peptide synthesis (SPPS) inside the silica mesoporous nanoparticles ²²⁻²⁴. They exhibited the capacity to monitor chemical changes occurring on the pore surface and modifications in the material's pore properties throughout each of the

successive functionalization steps. Moreover, they achieved the synthesis of the desired peptide sequence by employing a sequential coupling process for each amino acid. This method eliminates the requirement for the costly resin utilized in traditional SPPS and enables precise arrangement of amino acids, resulting in a high degree of functionalization of 2.1 ± 0.2 molecules/nm² ²². The chemical functionalities present on the channel surface play a pivotal role in determining the selectivity of the material ²⁵. While ceramic porous peptide hybrid materials have been synthesized using different approaches, especially the sequential grafting of amino acids bares the potential for highly precise peptide sequence and material property design going beyond sequence control of classical polymerization ^{26, 27}.

Due to their pore size being within the Debye Screening Length, mesoporous materials have the ability to effectively regulate the accessibility of charged species by precisely controlling the charge and isoelectric point ²⁸. Thereby, external parameters have been demonstrated to control ionic nanopore accessibility, and external stimuli have been shown to gate nanopore accessibility in time. Azzaroni et al. as well as Silies et al. have explored the influence of ion type on (2-methacryloyloxy)ethyltrimethylammonium-modified surfaces and mesopores showing contact angle variation from hydrophilic to hydrophobic by changing the electrolyte counterion from chloride to azide ^{29, 30}. Interestingly, the ion type as well determines ionic mesopore accessibility from accessible pores to almost ion exclusion ³⁰⁻³⁴. With respect to polymer chain functionalization, it has been demonstrated within the last few years that the nanopore accessibility can be gradually controlled by precisely adjusting the polyelectrolyte amount, and polymer chain sequence and thus the charge density within the pore. The nanopore accessibility can be gradually controlled by precisely adjusting the polyelectrolyte amount and thus the charge density within the pore ³⁵⁻³⁹. Furthermore, Förster et al. carried out the functionalization of mesoporous films with various polymers, employing an adjustable

quantity of polymers through an automated procedure utilizing visible-light induced, controlled photoelectron/energy transfer-reversible addition-fragmentation chain-transfer (PET-RAFT) polymerization⁴⁰. In a previous study from our research group, Brilmayer et al. functionalized mesoporous silica films using responsive and orthogonally charged block-copolymers demonstrating chain sequence control in nanoscale pores. Grafting the copolymer 2-(dimethylamino)ethyl methacrylate)-block-2-(methacryloyloxy)ethyl phosphate (PDMAEMA-*b*-PMEP), this block copolymer shows pH-dependent transition from an anion- to a cation selective nanopore and does not indicate a zwitterionic charge at a pH at which both blocks should be charged³⁶. Ion exclusion as observed for nanoscale pores functionalized with zwitterionic polymers carrying a negative and a positive charge within each monomer, such as PCBMA, was not observed⁴¹. This indicates the influence of polymer chain architecture on ionic nanopore accessibility and mass transport⁴¹. In a study by Szleifer et al., successful nanogating and transport direction was demonstrated by attaching a block of weak polyelectrolyte polymer with a precise assembly of polar and unpolar monomer sequences to the inner surface of the nanopore⁴². This theoretical study suggests that a precise design of polymer sequences, combining charged hydrophilic and neutral hydrophobic motifs into separate blocks, could be a general principle for constructing smart nanopores⁴². The proposed design implies that even more precise polymer chain sequence control, as achieved by classical radical polymerization, is of interest for nanopore transport design.

Here, we used direct in-pore solid-phase ultra-short peptide synthesis in mesoporous silica films to investigate amino acid functionalization and sequence control and its impact on ionic mesopore accessibility (Scheme 1). Mesoporous silica films are functionalized by arginine, leucine, and glycine amino acid grafting. Up to 5 cycles in arginine grafting, a stepwise increase of positive charge is expected at pH 3. Despite relatively low amounts of detected amino acid,

ion transport was controlled by adjusting the sequence and charge of peptide and functional mesoporous films. Thus, direct in-pore solid-phase ultra-short peptide synthesis on mesoporous films shows great potential for precise peptide sequence design and thus molecular transport control through such pores.

EXPERIMENTAL SECTION

Materials

The materials were purchased from Sigma-Aldrich. Methyl magnesium chloride in 3M Tetrahydrofuran (THF), 3-ethyl-2,4-dimethyl-pyrrole (97%), glutaric anhydride (95%), boron trifluoride-diethyl etherate ($\text{BF}_3 \cdot \text{OEt}_2$), triethylamine (Et_3N), N-bromosuccinimide (NBS, 99%), Dichloromethane (DCM), and sodium azide (NaN_3 , 99.5%) were used without any modifications. Pluronic® F-127, ethanol (EtOH) emplura, and tetraethyl orthosilicate (TEOS) were utilized for Evaporation-Induced Self-Assembly (EISA). The compound [3-(2-propynylcarbamate)propyl]triethoxysilane (PTEOS, 90%) was acquired from Gelest. Copper sulfate pentahydrate, (+)-sodium-L-ascorbate, Dimethyl sulfoxide (DMSO), Dimethylformamide (DMF) peptide grade, O-(Benzotriazol-1-yl)-N,N,N',N'-tetramethyluronium-hexafluorophosphat (HBTU, 98%), N, N-diisopropylethylamine (DIPEA), and various amino acids like Fmoc-Glycine, Fmoc-Arginine, and Fmoc-Leucine were applied to functionalize the films.

Dye synthesis (BODIPY-COOH). As inspired by Williams et al ⁴³ the reaction was carried out. Methyl magnesium chloride (0.66 mL, 1.98 mmol) was added to 3-ethyl-2,4-dimethyl-pyrrole

(0.2428 mL and 1.8 mmol) in THF (4 mL) under inert atmosphere. The mixture was heated under reflux and under an inert atmosphere at 80-88 °C for 30 min` in an oven-dried flask with a stirrer. After cooling to room temperature, glutaric anhydride (0.128 g and 1.12 mmol) dissolved in anhydrous THF (1 mL) was added, followed by the gradual addition of $\text{BF}_3 \cdot \text{OEt}_2$ (0.399 mL, 0.459 g and 3.24 mmol). After stirring for 18 hours, triethylamine (1.536 mL, 1.122 g, and 12 mmol) and $\text{BF}_3 \cdot \text{OEt}_2$ (1.10 mL, 1.27 g, and 9 mmol) were added and stirred at 50 °C for 4 hours. The reaction was quenched with a solution of ammonium chloride, and the residual precipitate was dissolved in DCM before being combined with the reaction mixture. The mixture was then extracted with DCM and washed with water three times (15 mL each) (3 x 100 mL). The organic layer was dried over MgSO_4 , and the solvent was evaporated overnight under a vacuum. The resulting residue was further purified by TLC (hexane/EtOAc/HOAc, 80:40:1) via column chromatography. The reaction progress and the determination of the solvent mixture used for column chromatography were monitored by TLC. The solvent system had the R_f value of 0.31, yielding 37% (130 mg) of red solid BODIPY-COOH. ^1H , and ^{13}C NMR spectra are depicted in Figure S1, and S2.

Dye synthesis (BODIPY-N3). The reaction was carried out in accordance to Strasser et al.⁴⁴ under a nitrogen atmosphere in the absence of light. BODIPY-COOH (0.117 g, 0.299 mmol, 1 eq.) was dissolved in 3 mL of dry DCM, followed by the addition of NBS (53 mg, 0.298 mmol, 1 eq.) in 3 mL DCM. The reaction mixture was stirred for 1 hour at room temperature in the dark. Then, 150 mg of NaN_3 suspended in 3 mL of dry DMF was added, and the reaction was allowed to proceed in the dark for 2 hours. The resulting product was dissolved in 30 mL of Ethyl acetate (EtOAc) and washed with brine. After drying the organic phase over MgSO_4 , the solvent was evaporated under reduced pressure, and the crude product was purified using

column chromatography (hexane/EtOAc/HOAc, 80:40:1), yielding a red-orange solid with a 30.76 % yield with the R_f value of 0.72 (Figure S3).

Mesoporous Silica Film Preparation. Mesoporous silica films were prepared by sol-gel chemistry and EISA using TEOS and Pluronic F127 as a mesopores-forming template. Regarding the dip-coating solution, 9.8 mL of TEOS were dissolved in 48.0 mL of ethanol. Afterward, 5.22 g of Pluronic F127 and 12.8 mL of a recently prepared hydrochloric acid solution (0.05 M) were introduced. The solution was stirred for 1 hour at room temperature and was subsequently stored in a freezer at -18°C until it was ready for application. These precursor solutions are applied to a dip-coating process and EISA on a silicon wafer, glass, or indium tin oxide (ITO)-coated glass substrate at 49-50% relative humidity and 298 K, using a withdrawal speed of 2 mm/s. Once the coating is completed, the films are kept at 50% relative humidity for 1 h. Subsequently, a heat treatment is carried out in two steps lasting 1 h each at 60 and 130 $^{\circ}\text{C}$ to stabilize the film. Finally, the temperature was gradually increased at a rate of 1 $^{\circ}\text{C}/\text{min}$ until it reaches 350 $^{\circ}\text{C}$, where it is kept for two hours before cooling down to ambient temperature.

Surface grafting of PPTEOS. The surface grafting of PPTEOS onto the mesoporous silica film was carried out under a nitrogen atmosphere. A dry, three neck, round-bottomed flask with a volume of 250 mL was filled with 4.4 μL of NEt_3 (0.23 eq., 0.032 mmol) dissolved in 230 mL of anhydrous toluene. An excess amount of PPTEOS (1 eq., 0.141 mmol, 45 μL) was added to the agitated mixture. Subsequently, 100 mL of this reaction mixture were transferred to the Schlenk flask containing eight, priority de-gassed, glass substrates coated with mesoporous silica. The reaction mixture was stirred at 60 $^{\circ}\text{C}$ for 5 h and then heated to 100 $^{\circ}\text{C}$ under reflux and under an inert atmosphere for 3 h. PPTEOS demonstrates a comparatively lower

reactivity. To enhance its reactivity, we employ elevated temperatures. This process is facilitated using a balloon apparatus. The thin films were washed and extracted with toluene to remove any contaminants.

Conjugation of BODIPY-N3 into the films via click chemistry reaction. The reaction to conjugate BODIPY-N3 to the PTEOS functionalized mesoporous silica films were carried out in the dark under a nitrogen atmosphere. First, copper sulfate pentahydrate (0.1 mmol, 26 mg) and (+)-sodium-L-ascorbate (0.15 mmol, 30 mg) were mixed in 2-3 mL of Milli-Q water. Then, BODIPY-azide (15 mg) was dissolved in 6 mL of DCM and 230 mL of DMSO. The solution was added to mesoporous films under protective (dry and oxygen-free) nitrogen atmosphere. The reaction mixture was stirred overnight, and the substrates were washed and extracted in ethanol for 30 minutes before being dried.

General procedure for the synthesis of the peptide into the pore of the mesoporous silica film. The mesoporous film-coated substrates were placed in Schlenk flask containing 100 mL of DMF. HOBt (0.1 eq., 0.45 mmol, 61.8 mg) was dissolved in a minimum of 2 mL of DMF, and then HBTU (0.5 eq., 2.1 mmol, 0.8 g) was added. Subsequently, 6 mL of DMF containing 1 equivalent each of deprotected amino acid (4.26 mmol, 0.3 g) and DIPEA (3 eq., 12.8 mmol, 2.24 mL) were added to the reaction solution, resulting in a brown-coloured mixture. The reaction was continuously shaken at room temperature for 24 h. Subsequently, the film was washed and extracted with DMF. The same method was used to attach more amino acids (such as arginine, glycine, and others) to the pore wall and improve the sequence of the short peptide.

Proton, Carbon, and Boron Nuclear Magnetic Resonance (^1H , ^{13}C) Spectroscopy. The characterization of all produced compounds was carried out using Proton, Carbon, and Boron Nuclear Magnetic Resonance (^1H , and ^{13}C) spectroscopy. A Bruker DRX 500 or a Bruker AC 300

spectrometer was used. A sample concentration of 10 mg of a substance per 1 mL of a deuterated solvent was used for ^1H -NMR, and ^{13}C -NMR measurements. MestReNova was utilized to analyse all NMR spectra.

Fluorescence Spectroscopic Measurements. The fluorescence emission spectra were obtained upon excitation at 480 nm and measuring emissions between 500 to 650 nm using a fluorescence spectrofluorometer (FLUOROMAX_PLUS_C_0587D-2722-FMPLUS). The measurements were recorded by placing 2 mL of each sample in a quartz cuvette, with the excitation and emission set at 90° , and the integration time was set to 0.1 s.

Cyclic voltammetry (CV). To assess the ionic permselectivity of mesoporous materials, cyclic voltammetry (CV) was conducted. A supporting electrolyte of 100 mM aqueous KCl and 2 mM $[\text{Fe}(\text{CN})_6]^{3-/4-}$ or $[\text{Ru}(\text{NH}_3)_6]^{2+/3+}$ was used. The pH was adjusted to acidic or basic adding drops of HCl 0.1 M or NaOH 0.1 M to a volume of 25 mL of the aqueous KCl solution containing the redox-active probe molecule, $[\text{Fe}(\text{CN})_6]^{3-/4-}$ or $[\text{Ru}(\text{NH}_3)_6]^{2+/3+}$. Mesoporous silica films were fabricated on glass substrates coated with ITO (Delta Technologies, 4-8 Ω) were employed as the working electrode. The reference electrode employed was an Ag/AgCl electrode (BASi, Type RE-6), and the counter electrode used was a graphite electrode (Alfa Aesar). A series of scan rates between 200 and 100 mV/s, each one cycled three times, was recorded. The cyclic voltammograms were recorded with an Autolab PGSTAT302N. The data was rigorously monitored for quality by comparing the scan rate of 200 mV/s at the beginning and at the end of each scan rate cycle. The data was only analysed further in case both scans were comparable.

Attenuated Total Reflectance–Infrared Spectroscopy. IR spectra were acquired from Perkin-Elmer in the mid-IR range of 4000-650 cm^{-1} using attenuated total reflectance–infrared spectroscopy (ATR-IR) mode. After automatic background correction, the spectra were normalized to the Si-O-Si asymmetric stretching vibrational band at 1080 cm^{-1} . The samples were scratched off the substrate using a razor blade.

Contact angle. The Dataphysics Instruments GmbH model TBU90E, along with the SCA-Software application, was utilized to measure macroscopic static contact angles. A water droplet volume of 2 μL was applied (dispensing rate: 1 $\mu\text{L s}^{-1}$) for macroscopic static contact angle measurements.

Ellipsometry. To measure the thickness and the refractive index of mesoporous silica films on silicon wafer substrates (Si-Mat, Kaufering, Germany, 100mm diameter, 525±25 μm thickness, type P/Bor, orientation, CZ growth method, 2–5W resistivity, polished on 1 side), the Nanofilm EP3-SE imaging ellipsometer from the company ACCURION was used. The measurements were recorded using a 658 nm laser with a single zone angle of incidence (AOI) variation measurement between AOIs of 38 and 70° in 2° increments. The relative humidity was kept at 15% by using humidity management and the program Regul'Hum (SOLGELWAY, Sceaux, France, version 3.3). The software EP4-View and EP4-Model (Accurion GmbH, Goettingen, Germany, version 1.2.0) were employed for both measurement and model analysis. These measurements were carried out at three specific points along the direction of dip coating and were performed in a one-zone mode, encompassing the sequence silicon wafer to SiO_2 oxide layer to SiO_2 mesoporous structure. Bruggemann's effective medium theory^{45, 46}, was used to determine pore filling based on refractive indices.

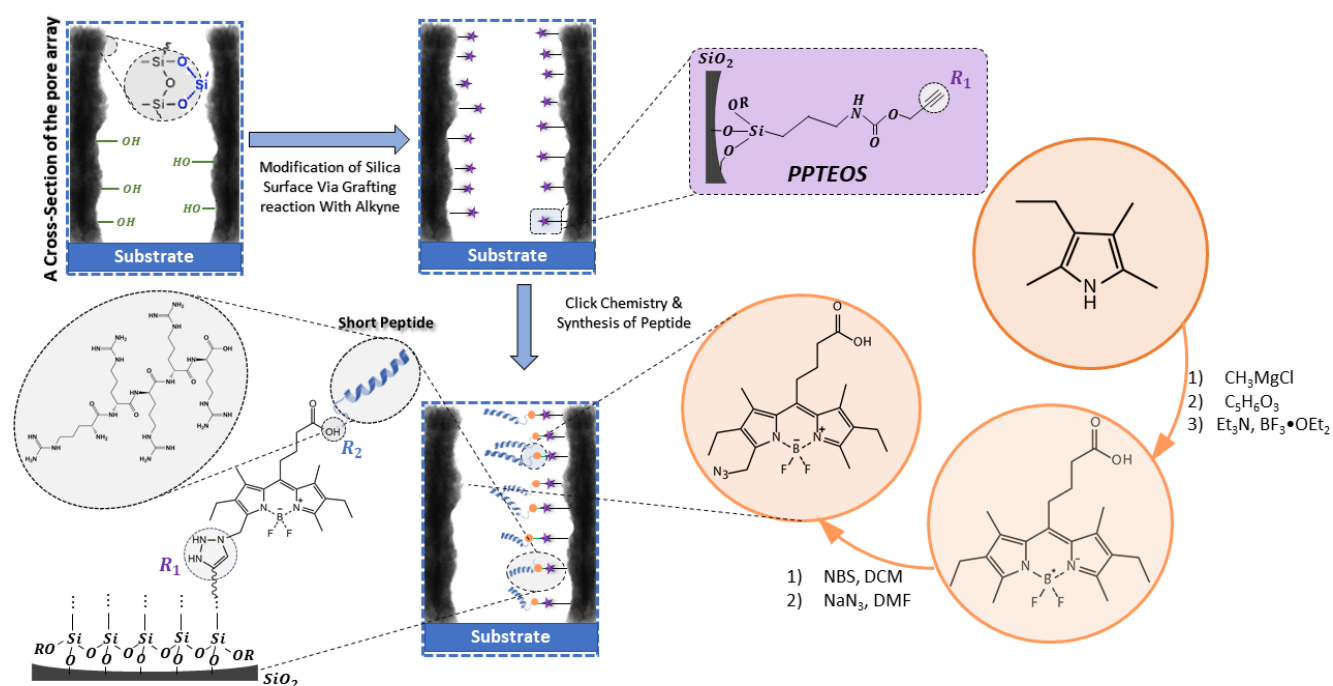
UV/VIS-spectroscopy. UV/VIS spectra were recorded using an Agilent Cary 60 UV-Vis spectrometer and the Agilent Cary WinUV-Software. Before each measurement, the background was corrected by performing a scan in air without any sample present.

RESULTS AND DISCUSSION

Mesoporous silica films were prepared using sol-gel chemistry and EISA according to a protocol of Dunphy et. al.⁴⁷. The obtained mesoporous films show film thickness of 640 nm and a porosity of 52 vol % which were obtained from ellipsometry results (Figure 1c) using the effective medium approximation⁴⁵. PPTEOS was grafted to the mesoporous silica films to allow for subsequent conjugation reactions to the PPTEOS alkyne group (Scheme 1). Upon PPTEOS grafting, the refractive index increases from 1.214 to 1.269 indicating a pore filling of around 22 vol% (Figure 1c).

It has to be noted that the applied silane, PPTEOS, contains three ethoxy anchor groups per silane, indicating the potential for multilayer formation due to three anchor groups per silane. ATR-IR spectra support successful PPTEOS grafting based on the C=O vibrational band at 1710 cm^{-1} (Figure 1a). Subsequent conjugation of BODIPY-N3 using click chemistry results in the further refractive index increase of up to 1.315, indicating an increase in pore filling up to 40 vol %. Bodipy-N3 conjugation additionally results in a new vibrational band in the ATR-IR spectra at 1680 cm^{-1} assigned to the ester C=O vibration. In addition, the stretching vibrational band assigned to the BODIPY C=N bond⁴⁸ appeared at 1549 cm^{-1} as well indicating successful BODIPY functionalization. Furthermore, the fluorescence intensity increased,

indicating the presence of BODIPY (Figure 1f). Amino acid binding to the BODIPY is carried out by immersing PTEOS- and BODIPY-functionalized mesoporous silica films under continuous agitation at room temperature into the DMF solution containing the deprotected amino acids and the coupling reagents (Scheme 1). Upon peptide conjugated to the mesoporous films, the ATR-IR spectra show a vibrational band at 1660 cm^{-1} , which is attributed to the amide bond (amide I) in accordance with literature ^{17, 49-51} (Figure S4).

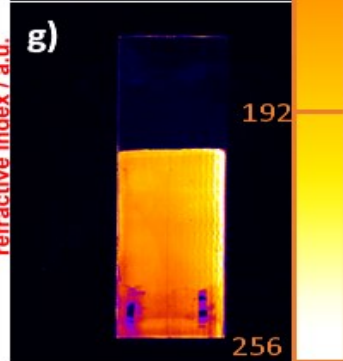
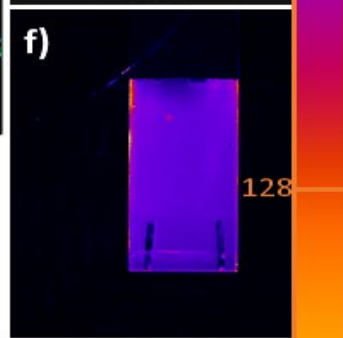
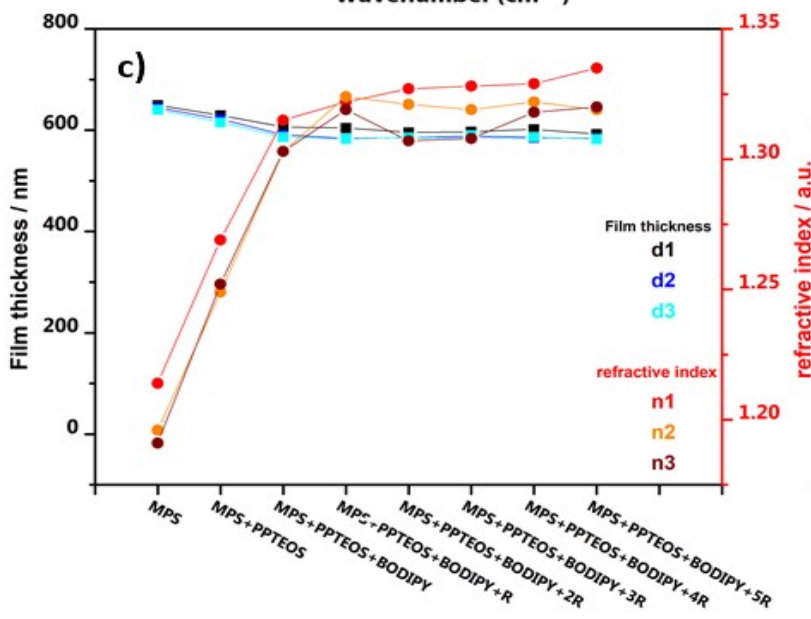
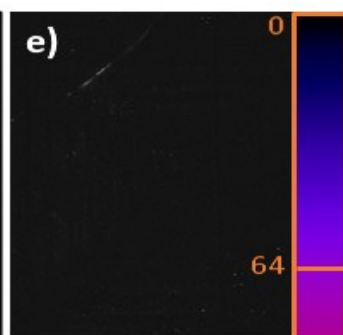
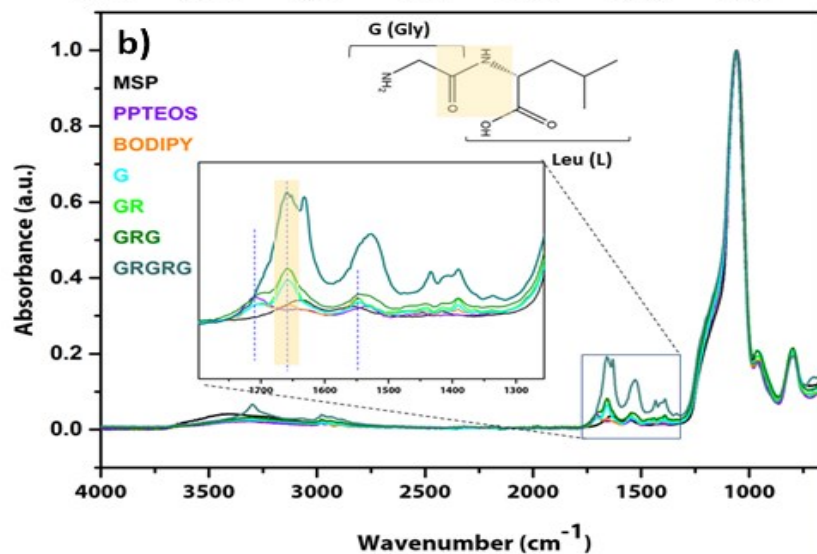
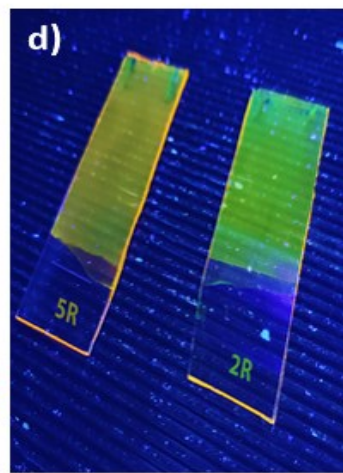
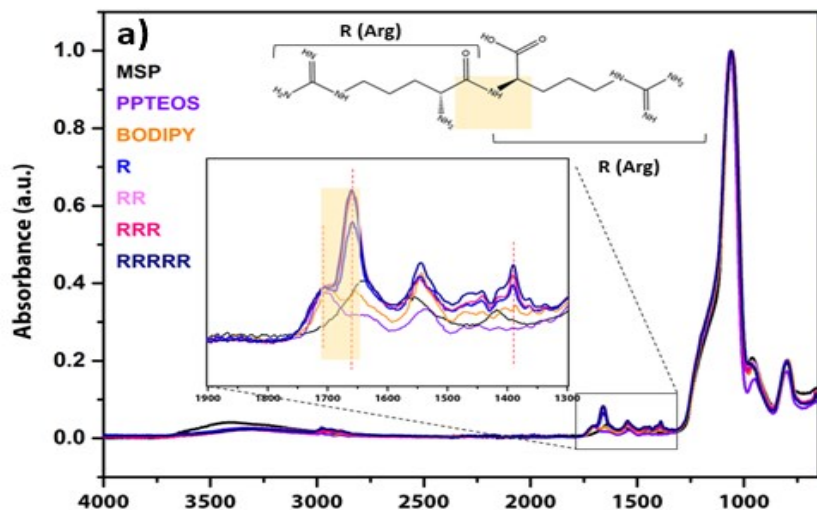


Scheme 1. Functionalized Silica Mesoporous Film with a variety of materials.

Various peptide sequences based on glycine (G), leucine (L), and arginine (R), including R up to 5R, G, GR, GRG, GRGRG, GGG, GL, and GLGL, were grafted from the mesoporous films, and characterized for their presence after completion of the grafting reaction. Glycine and leucine were selected for its neutral charge, whereas arginine was selected for its positive charge. The ATR-IR spectra obtained from the mesoporous silica films before and after amino acid

grafting indicate successful peptide grafting from the mesoporous films for glycine, leucine, and arginine (Figure 1a,b). The representative spectra shown in Figures 1a,b were normalized to the asymmetric Si-O-Si stretching vibrational band at 1080 cm^{-1} . The unfunctionalized mesoporous film (Figure 1, black) did not exhibit a vibrational band associated to PPTEOS, BODIPY or peptide grafting at 1710 cm^{-1} , 1680 cm^{-1} or 1660 cm^{-1} . Upon arginine grafting, the ATR-IR spectra (Figure 1a,b) indicate increasing intensity of the amino acid-related C=O stretching vibration at 1660 cm^{-1} , in accordance with the literature ⁵¹. Furthermore, an increase in the refractive index from 1.315 to 1.335 is observed indicating a total pore filling of 48 vol % upon amino acid grafting (Figure 1c). The functionalization of silica mesopores with peptides depends on the specific amino acid employed. This dependence of the grafted amino acid amount on the type of selected amino acid seems to be influenced by the amino acid charge. With increasing number of amino acid binding cycles such as GGG, GRGRG, and GLGL sequences, we observe an increase in the C=O stretching vibration of amino acids at 1660 cm^{-1} . It has to be noted that the magnitude of this increase fluctuates depending on the particular amino acid sequence. In the case of grafting the RRRRR sequence, it becomes evident that the C=O stretching vibrational band does not further increase after two binding steps. This observation may be related due to the increasing positive charge with increasing number of grafted arginine molecules (Figure S6). Interestingly, the fluorescence spectra of BODIPY, 2R, and 5R samples displayed one primary fluorescence emission between 500 and 650 nm with a maximum at 530 nm (Figure S10). However, the fluorescence intensity at 530 nm increased and exhibited a broader peak that extended into the red after grafting arginine in five subsequent steps (5R sample) as compared to that of the 2R sample. This observation was corroborated by the UV images of the 5R and 2R samples, which were orange and green in color (Figure 1d). As a reference, the mesoporous silica film functionalized with BODIPY was

placed into a solution without peptide, and subsequently examined for its fluorescence properties. As no change in the fluorescence intensity was observed the different fluorescence spectra are ascribed to the arginine grafting. The fluorescence wavelength and intensity change upon peptide grafting to BODIPY are in agreement with literature as the peptide binding affects HOMO and LUMO energy levels^{52,53}. Thus, the observed fluorescence intensity changes upon amino acid grafting as well as supports successful grafting of amino acid into the BODIPY-functionalized silica mesopores. Thereby, the macroscopic static contact angle of all samples remains hydrophilic between 58 and 38° (Figure S9).



Fluorescence Intensity x32 pixels; 8-bit; 8K

Figure 1. (a, b) ATR-IR spectra of mesoporous silica film (black), PTEOS (purple), BODIPY (orange), Arginine, R (blue), Glycine, G (cyan), RR (light pink), GR (light green), RRR (dark pink), GRG (dark green), RRRRR (navy blue), and GRGRG (dark turquoise), (c) ellipsometry results of refractive index (red) and film thickness (black) at 15% relative humidity, (d) Photo of samples with two and five sequences of arginine under UV lamp, fluorescence's images with using an excitation wavelength of 530 nm of (e) Mesoporous silica film, MSP; (f) film with BODIPY functionalization; (g) film with 5R grafting.

To investigate the influence of amino acid functionalization on the pH-dependent ionic mesopore accessibility of mesoporous silica films, cyclic voltammograms of PTEOS, BODIPY, and glycine- and arginine-functionalized mesoporous silica films were recorded using $[\text{Fe}(\text{CN})_6]^{4-/3-}$ and $[\text{Ru}(\text{NH}_3)_6]^{2+/3+}$ as redox-active probe molecule. Upon PTEOS grafting (Figure 2, violet), a decrease in $[\text{Fe}(\text{CN})_6]^{4-/3-}$ and $[\text{Ru}(\text{NH}_3)_6]^{2+/3+}$ peak current density for all probe molecules and for all pH values as compared to unmodified mesoporous silica was observed, which correlates to the increased pore filling. While the peak current density for $[\text{Ru}(\text{NH}_3)_6]^{2+/3+}$ and $[\text{Fe}(\text{CN})_6]^{4-/3-}$ in unmodified mesoporous silica films (Figure 2, black) at acidic pH is very low, it is almost zero for $[\text{Fe}(\text{CN})_6]^{4-/3-}$ at basic pH. This indicates the electrostatic exclusion at basic pH due to remaining deprotonated silanol groups at the mesopore wall. This electrostatic exclusion of $[\text{Fe}(\text{CN})_6]^{4-/3-}$ is in accordance with a significant $[\text{Ru}(\text{NH}_3)_6]^{2+/3+}$ cation preconcentration at basic pH (Figure 2f, purple).

Subsequent BODIPY functionalization (Figure 2b) causes an increase in I_p for $[\text{Ru}(\text{NH}_3)_6]^{2+/3+}$ (Figure 2, orange) and an almost constant I_p for $[\text{Fe}(\text{CN})_6]^{4-/3-}$ as compared to PTEOS-functionalized films. Thereby, the I_p is still significantly lower as compared to unmodified mesoporous silica films. Furthermore, at basic solution pH (Figure 2d,f, orange), the accessibility of cations is increased as compared to pH 3 (Figure 2d, orange) indicating the presence of the negatively charged BODIPY together with the remaining deprotonated silanol

groups at basic pH. Thus, the ionic mesopore accessibility shows accessible mesopores and expected electrostatically controlled ionic mesopore accessibility after both PTEOS and BODIPY grafting. The pore filling degrees in the range of 40 vol % according to ellipsometry (Figure 1c) do not prevent mesopore accessibility.

Subsequent amino acids grafting of glycine and arginine, which carry neutral and positive charges, further supports this electrostatic control. Arginine grafting introduces a positive charge at acidic pH. This positive charge leads to a decrease in the maximum peak current density for the positively charged $[\text{Ru}(\text{NH}_3)_6]^{2+/3+}$ at pH 3 as compared to the glycine-functionalized film (Figure 2e, blue vs cyan). Although the lower peak current density observed for arginine in comparison to glycine-functionalized mesopores suggests reduced accessibility of the cationic $[\text{Ru}(\text{NH}_3)_6]^{2+/3+}$ probe molecule due to the positive charge of arginine at pH 3, the $[\text{Ru}(\text{NH}_3)_6]^{2+/3+}$ can still significantly access the mesopores (Figure 2e, blue). Thus, no complete electrostatic pore blocking occurs. At pH 10, both, arginine as well as glycine-functionalized mesoporous silica films exclude anionic $[\text{Fe}(\text{CN})_6]^{4-/3-}$ probe molecules indicating the influence of deprotonated silanol groups at the mesopore walls (Figure 2d). This is supported by the I_p for $[\text{Ru}(\text{NH}_3)_6]^{2+/3+}$ at basic pH which is slightly reduced as compared to acidic pH but still indicates significant mesopore accessibility (Figure 2f). Especially the ionic mesopore accessibility for $[\text{Fe}(\text{CN})_6]^{4-/3-}$ at acidic pH indicates the presence of arginine and glycine. Nevertheless, at basic pH, the remaining deprotonated silanol groups dominate mesopore accessibility. Thus, the grafted number of R and G seems to be relatively low which is consistent with the minimal change in refractive index after grafting amino acid and ATR-IR results.

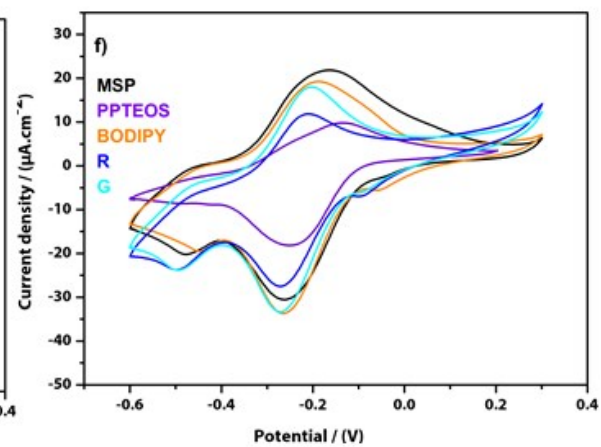
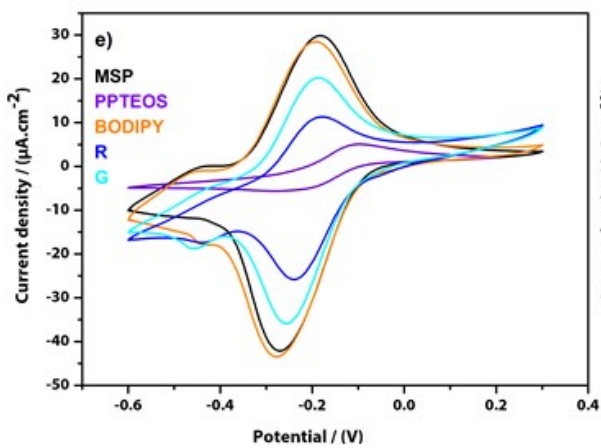
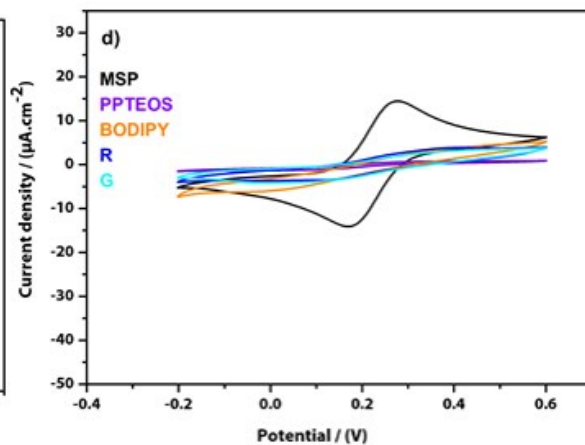
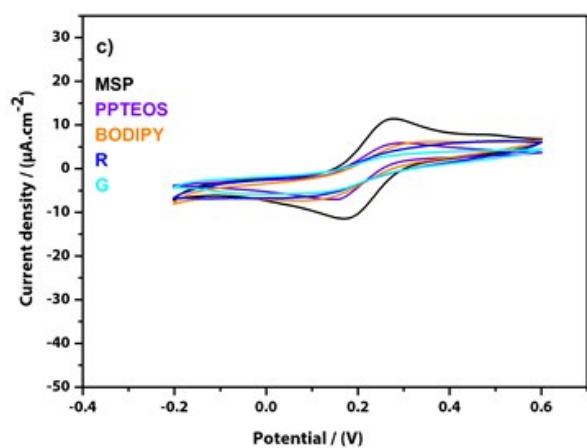
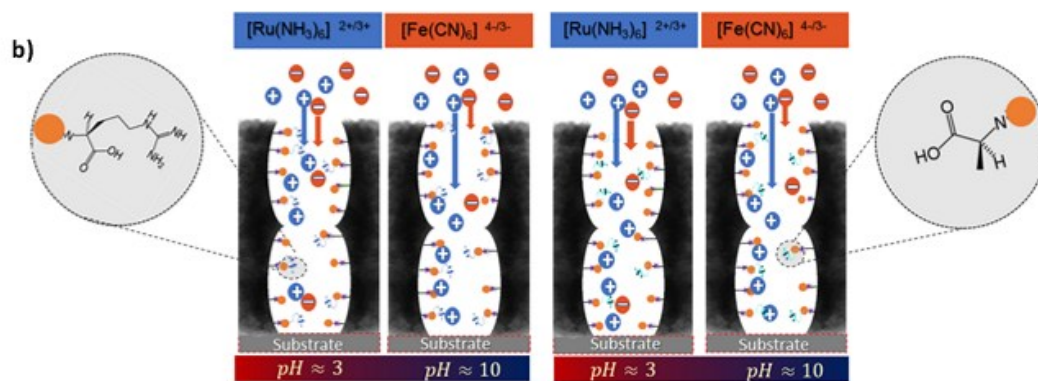
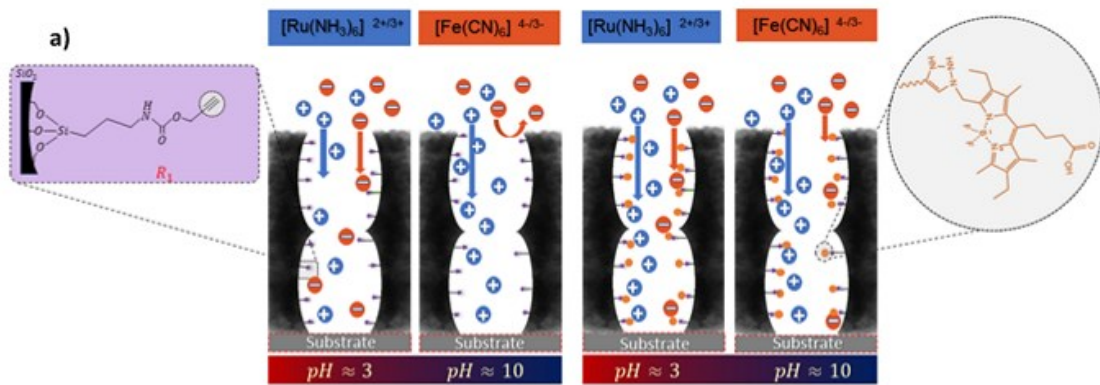


Figure 2. Cyclic voltammetry at an ITO electrode below the mesoporous film (black) with different functional group like a) PTEOS (purple), and BODIPY as a photolinker (orange), b) one sequence of arginine (R - blue line), and one sequence of glycine (G - cyan) at c) pH 3, $[\text{Fe}(\text{CN})_6]^{3-/4-}$, d) pH 10, $[\text{Fe}(\text{CN})_6]^{3-/4-}$, e) pH 3, $[\text{Ru}(\text{NH}_3)_6]^{2+/3+}$, f) pH 10, $[\text{Ru}(\text{NH}_3)_6]^{2+/3+}$. Cyclic voltammograms are recorded at a scan rate of 100 mV s^{-1} in a 0.1 M KCl-solution.

Following the vision of the chain sequence design, the arginine binding cycles were increased up to 5R which resulted into slightly higher arginine amount as deduced from ATR-IR and ellipsometry (Figure 1 and S6) and thus into a slightly increasing positive charge density within the silica mesopore at pH 3 (Figure 3). This is expected to result into increasing electrostatic attraction of $[\text{Fe}(\text{CN})_6]^{4-/3-}$ probe molecules especially at acidic pH, while the cationic $[\text{Ru}(\text{NH}_3)_6]^{2+/3+}$ mesopore accessibility at acidic pH should be increasingly hindered. Indeed, the I_p for $[\text{Fe}(\text{CN})_6]^{4-/3-}$ at pH 3 is relatively small after one R functionalization but increases for 5R indicating increasing positive charge density even at the observed relatively low total amino acid amount within the mesopores (Figure 3b). Simultaneously, a decrease of I_p with an increasing number of positively charged arginine binding is observed for $[\text{Ru}(\text{NH}_3)_6]^{2+/3+}$. At an acidic pH, the increase in the charge density leads to electrostatic exclusion of identically charged ions from the mesopores (Figure 3d) after 5R functionalization.

When adapting the solution pH to basic 5R, displayed comparable maximum peak current densities when exposed to the cationic $[\text{Ru}(\text{NH}_3)_6]^{2+/3+}$ probe at pH 10 (Figure 3e). This similarity in current densities is attributed to the neutral charge of the arginine at pH 10 and potentially remaining accessible deprotonated silanol groups at the mesopore wall leading to comparable and silanol group dominated surface charge among the different sequences. The

influence of deprotonated silanol groups at basic pH is supported by the electrostatic exclusion of the negatively charged $[\text{Fe}(\text{CN})_6]^{4-/3-}$ probe molecule at basic pH (Figure 3c). The probe molecule exclusion indicates the resilience of mesopores to significant degradation under the applied conditions (Figure 3c).

Interestingly, despite the apparently low amount of amino acid within the mesopores, a clear effect due to the increase of positive charge density within the mesopores with increasing arginine binding cycles of up to 5R is observed at acidic pH, while at basic pH, the remaining silanol groups dominate the ionic pore accessibility. This indicates the sensitive charge regulation in nanoscale pores. Thus, by using peptide functionalization allowing, in general, highly precise chain sequence control, the pore charge was pH-dependently switched from positive at acidic pH to negative at basic pH.

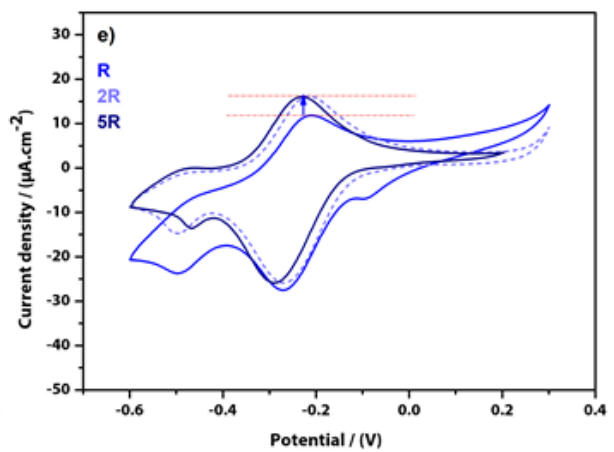
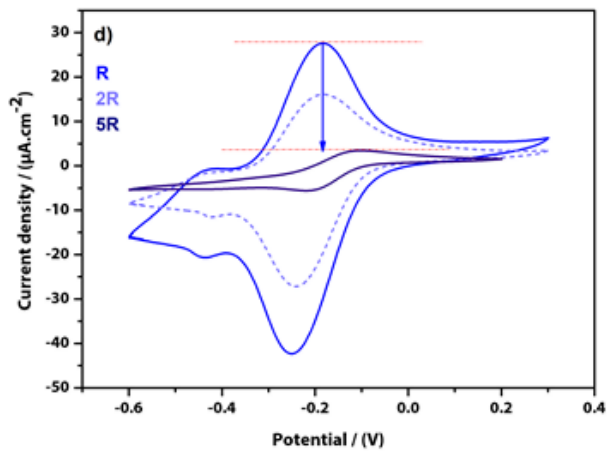
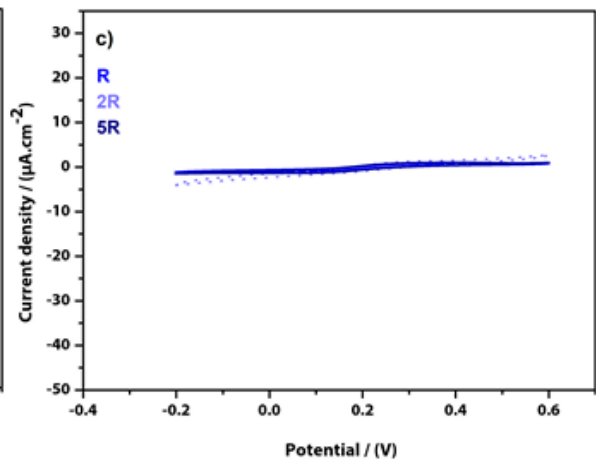
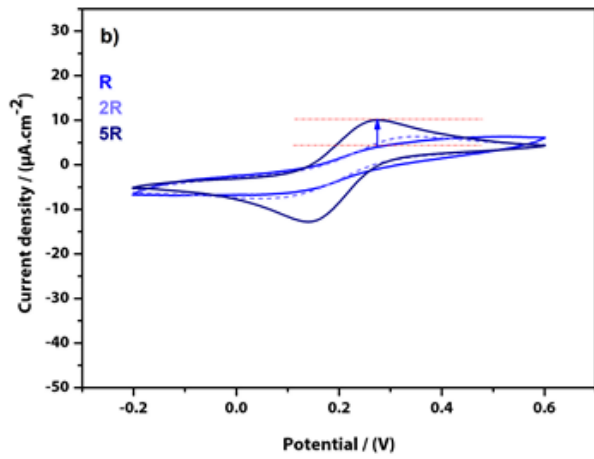
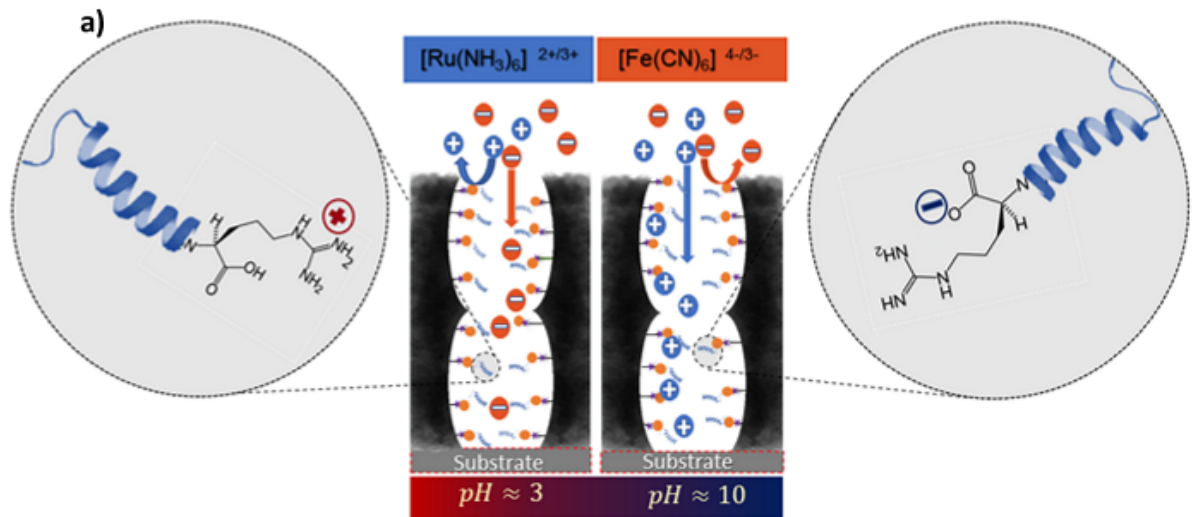


Figure 3. Cyclic voltammetry at an ITO electrode below the mesoporous film with different arginine cycle binding like R (blue), 2R (light blue), and 5R (navy blue) at b) pH 3, $[\text{Fe}(\text{CN})_6]^{3-/4-}$, c) pH 10, $[\text{Fe}(\text{CN})_6]^{3-/4-}$, d) pH 3, $[\text{Ru}(\text{NH}_3)_6]^{2+/3+}$, e) pH 10, $[\text{Ru}(\text{NH}_3)_6]^{2+/3+}$. Cyclic voltammograms are recorded at a scan rate of 100 mV s^{-1} in a 0.1 M KCl -solution).

CONCLUSION

In conclusion, direct in-pore solid-phase ultra-short peptide synthesis in mesoporous films was demonstrated for creating functional materials. For example, the pH-dependent positively charged amino acid arginine was covalently grafted from mesoporous films via PPTEOS and BODIPY. The successful functionalization of the films with PPTEOS, BODIPY, and different peptide sequences was confirmed through ATR-IR spectroscopy and ellipsometry showing a relatively low increase of pore filling (from 40 to 48 vol %) upon arginine functionalization. Nevertheless, cyclic voltammetry experiments revealed pH- and arginine-amount-dependent ionic mesopore accessibility. Thus, charge regulation in dependence on arginine binding cycles and pH was achieved even at low arginine amount, indicating the potential of precise chain sequence control possible by using peptide chemistry.

AUTHOR INFORMATION

Corresponding Author:

Annette Andrieu-Brunsen, Department of Chemistry, Technical University of Darmstadt, Peter-Grünberg-Str. 4, 64287 Darmstadt, Germany. E-mail: annette.andrieu-brunsen@tu-darmstadt.de, Orcid.org/ 0000-0002-3850-3047

Author:

Mohadeseh Bagherabadi, Department of Chemistry, Technical University of Darmstadt, Peter-Grünberg-Str. 4, 64287 Darmstadt, Germany. Orcid.org/ 0000-0001-9031-5281

Author Contributions

‡All authors have given approval to the final version of the manuscript.

Notes

The authors declare no competing financial interest.

Supporting Information.

Characterization of BODIPY synthesis, ¹H NMR and ¹³C NMR of BODIPY-COOH, ATR-IR of BODIPY-N₃, ATR-IR from reference samples, Macroscopic static contact angle, Fluorescence spectrum of samples with BODIPY.

ACKNOWLEDGMENTS

This project has received funding from the European Union's Horizon 2020 research and innovation programme under the Marie Skłodowska-Curie grant agreement No. 955664 (STIMULUS). Furthermore, the authors would like to express their gratitude to Prof. Dr. Nico Bruns (Chemistry Department, TU-Darmstadt) for access to fluorescence spectroscopy, to Prof. Dr. Katja Schmitz (Chemistry Department, TU-Darmstadt) for access to freeze drying equipment, and to Prof. Dr. Markus Biesalski (Chemistry Department, TU-Darmstadt) for

providing access to characterization facilities. The authors also thank Dr. Olga Avrutina (research group Prof. Kolmar, Chemistry Department, TU-Darmstadt) for fruitful discussions on peptide synthesis. The NMR and MS Departments are acknowledged for their assistance with measurements.

REFERENCES

1. Ovejero Paredes, K.; Díaz-García, D.; García-Almodóvar, V.; Lozano Chamizo, L.; Marciello, M.; Díaz-Sánchez, M.; Prashar, S.; Gómez-Ruiz, S.; Filice, M., Multifunctional Silica-Based Nanoparticles with Controlled Release of Organotin Metallo-drug for Targeted Theranosis of Breast Cancer. *Cancers* **2020**, *12* (1), 187.
2. de la Torre, C.; Agostini, A.; Mondragón, L.; Orzaez, M.; Sancenón, F.; Martínez-Mañez, R.; Marcos, M. D.; Amorós, P.; Pérez-Payá, E. J. C. c., Temperature-controlled release by changes in the secondary structure of peptides anchored onto mesoporous silica supports. *J Chemical communications* **2014**, *50* (24), 3184-3186.
3. Li, R.; Mei, X.; Li, X.; Zhang, C.; Ruan, L., A bolt-like-blocking nanovalve on mesoporous silica nanoparticles for controlled release. *Microporous and Mesoporous Materials* **2021**, *317*, 111007.
4. Zhao, J.-G.; Cao, J.; Wang, W.-Z., Peptide-Based Electrochemical Biosensors and Their Applications in Disease Detection. *Journal of Analysis and Testing* **2022**, *6* (2), 193-203.
5. Parandhaman, T.; Choudhary, P.; Ramalingam, B.; Schmidt, M.; Janardhanam, S.; Das, S. K., Antibacterial and Antibiofouling Activities of Antimicrobial Peptide-Functionalized Graphene–Silver Nanocomposites for the Inhibition and Disruption of *Staphylococcus aureus* Biofilms. *ACS Biomaterials Science & Engineering* **2021**, *7* (12), 5899-5917.
6. Apostolopoulos, V.; Bojarska, J.; Chai, T.-T.; Elnagdy, S.; Kaczmarek, K.; Matsoukas, J.; New, R.; Parang, K.; Lopez, O. P.; Parhiz, H. J. M., A global review on short peptides: Frontiers and perspectives. *Molecules* **2021**, *26* (2), 430.
7. Lu, L.; Duong, V. T.; Shalash, A. O.; Skwarczynski, M.; Toth, I. J. V., Chemical conjugation strategies for the development of protein-based subunit nanovaccines. *J Vaccines* **2021**, *9* (6), 563.
8. Zeng, L.; Liao, Z.; Li, W.; Yuan, Q.; Wu, P.; Gu, Z.; Liu, Z.; Liao, G. J. C. C. L., Non-covalent glycosylated gold nanoparticles/peptides nanovaccine as potential cancer vaccines. *J Chinese Chemical Letters* **2020**, *31* (5), 1162-1164.
9. Li, T.; Lu, X.-M.; Zhang, M.-R.; Hu, K.; Li, Z., Peptide-based nanomaterials: Self-assembly, properties and applications. *Bioactive Materials* **2022**, *11*, 268-282.
10. Iranmanesh, H.; Subhash, B.; Glover, D. J.; Bedford, N. M., Proteins and peptides for functional nanomaterials: Current efforts and new opportunities. *MRS Bulletin* **2020**, *45* (12), 1005-1016.
11. Tao, K.; Levin, A.; Adler-Abramovich, L.; Gazit, E., Fmoc-modified amino acids and short peptides: simple bio-inspired building blocks for the fabrication of functional materials. *Chemical Society Reviews* **2016**, *45* (14), 3935-3953.
12. Adler-Abramovich, L.; Gazit, E. J. C. S. R., The physical properties of supramolecular peptide assemblies: from building block association to technological applications. *J Chemical Society Reviews* **2014**, *43* (20), 6881-6893.
13. Ten Brummelhuis, N.; Wilke, P.; Börner, H. G. J. M. R. C., Identification of functional peptide sequences to lead the design of precision polymers. *J Macromolecular Rapid Communications* **2017**, *38* (24), 1700632.
14. Siegwart, D. J.; Oh, J. K.; Matyjaszewski, K., ATRP in the design of functional materials for biomedical applications. *Progress in Polymer Science* **2012**, *37* (1), 18-37.
15. von Baeckmann, C.; Rubio, G. M.; Kählig, H.; Kurzbach, D.; Reithofer, M. R.; Kleitz, F. J. A. C. I. E., Evaporation-Induced Self-Assembly of Small Peptide-Conjugated Silica Nanoparticles. *J Angewandte Chemie International Edition* **2021**, *60* (42), 22700-22705.
16. Jiang, H. S.; Zhang, Y.; Lu, Z. W.; Lebrun, R.; Gontero, B.; Li, W. J. S., Interaction between silver nanoparticles and two dehydrogenases: role of thiol groups. *J Small* **2019**, *15* (27), 1900860.
17. Mudakavi, R. J.; Vanamali, S.; Chakravorty, D.; Raichur, A. M. J. R. a., Development of arginine based nanocarriers for targeting and treatment of intracellular *Salmonella*. *J RSC advances* **2017**, *7* (12), 7022-7032.

18. Bartczak, D.; Kanaras, A. G., Preparation of Peptide-Functionalized Gold Nanoparticles Using One Pot EDC/Sulfo-NHS Coupling. *Langmuir* **2011**, *27* (16), 10119-10123.
19. Shen, W.-Z.; Cetinel, S.; Sharma, K.; Borujeny, E. R.; Montemagno, C., Peptide-functionalized iron oxide magnetic nanoparticle for gold mining. *Journal of Nanoparticle Research* **2017**, *19* (2), 74.
20. Liebes-Peer, Y.; Rapaport, H.; Ashkenasy, N., Amplification of Single Molecule Translocation Signal Using β -Strand Peptide Functionalized Nanopores. *ACS Nano* **2014**, *8* (7), 6822-6832.
21. Tsutsui, M.; Tanaka, M.; Marui, T.; Yokota, K.; Yoshida, T.; Arima, A.; Tonomura, W.; Taniguchi, M.; Washio, T.; Okochi, M. J. A. c., Identification of individual bacterial cells through the intermolecular interactions with peptide-functionalized solid-state pores. *J Analytical chemistry* **2018**, *90* (3), 1511-1515.
22. Brodrecht, M.; Breitzke, H.; Gutmann, T.; Buntkowsky, G. J. C. A. E. J., Biofunctionalization of Nano Channels by Direct In-Pore Solid-Phase Peptide Synthesis. *J Chemistry—A European Journal* **2018**, *24* (67), 17814-17822.
23. Brodrecht, M.; Kumari, B.; Thankamony, A. S. L.; Breitzke, H.; Gutmann, T.; Buntkowsky, G. J. C. A. E. J., Structural insights into peptides bound to the surface of silica nanopores. *J Chemistry—A European Journal* **2019**, *25* (20), 5214-5221.
24. de Oliveira, M.; Herr, K.; Brodrecht, M.; Haro-Mares, N. B.; Wissel, T.; Klimavicius, V.; Breitzke, H.; Gutmann, T.; Buntkowsky, G., Solvent-free dynamic nuclear polarization enhancements in organically modified mesoporous silica. *Physical Chemistry Chemical Physics* **2021**, *23* (22), 12559-12568.
25. Kim, S.; Nham, J.; Jeong, Y. S.; Lee, C. S.; Ha, S. H.; Park, H. B.; Lee, Y. J., Biomimetic Selective Ion Transport through Graphene Oxide Membranes Functionalized with Ion Recognizing Peptides. *Chemistry of Materials* **2015**, *27* (4), 1255-1261.
26. Zeng, Z.; Ai, Y.; Qian, S. J. P. C. C. P., pH-regulated ionic current rectification in conical nanopores functionalized with polyelectrolyte brushes. *J Physical Chemistry Chemical Physics* **2014**, *16* (6), 2465-2474.
27. Ali, M.; Nasir, S.; Ramirez, P.; Ahmed, I.; Nguyen, Q. H.; Fruk, L.; Mafe, S.; Ensinger, W. J. A. F. M., Optical gating of photosensitive synthetic ion channels. *J Advanced Functional Materials* **2012**, *22* (2), 390-396.
28. Schoch, R. B.; Han, J.; Renaud, P. J. R. o. m. p., Transport phenomena in nanofluidics. *J Reviews of modern physics* **2008**, *80* (3), 839.
29. Yameen, B.; Ali, M.; Álvarez, M.; Neumann, R.; Ensinger, W.; Knoll, W.; Azzaroni, O. J. P. C., A facile route for the preparation of azide-terminated polymers. "Clicking" polyelectrolyte brushes on planar surfaces and nanochannels. *J Polymer Chemistry* **2010**, *1* (2), 183-192.
30. Silies, L.; Gonzalez Solveyra, E.; Szleifer, I.; Andrieu-Brunsen, A., Insights into the Role of Counterions on Polyelectrolyte-Modified Nanopore Accessibility. *Langmuir* **2018**, *34* (20), 5943-5953.
31. Andrieu-Brunsen, A.; Micoureau, S. b.; Tagliazucchi, M.; Szleifer, I.; Azzaroni, O.; Soler-Illia, G. J. J. C. o. M., Mesoporous hybrid thin film membranes with PMETAC@ silica architectures: Controlling ionic gating through the tuning of polyelectrolyte density. *J Chemistry of Materials* **2015**, *27* (3), 808-821.
32. Wang, Z.; Yang, X.; Cheng, Z.; Liu, Y.; Shao, L.; Jiang, L. J. M. H., Simply realizing "water diode" Janus membranes for multifunctional smart applications. *J Materials Horizons* **2017**, *4* (4), 701-708.
33. Zhang, Z.; Wen, L.; Jiang, L. J. C. S. R., Bioinspired smart asymmetric nanochannel membranes. *J Chemical Society Reviews* **2018**, *47* (2), 322-356.
34. Siwy, Z. S. J. A. F. M., Ion-current rectification in nanopores and nanotubes with broken symmetry. *J Advanced Functional Materials* **2006**, *16* (6), 735-746.
35. Silies, L.; Didzoleit, H.; Hess, C.; Stühn, B.; Andrieu-Brunsen, A., Mesoporous Thin Films, Zwitterionic Monomers, and Iniferter-Initiated Polymerization: Polymerization in a Confined Space. *Chemistry of Materials* **2015**, *27* (6), 1971-1981.
36. Brillmayer, R.; Hess, C.; Andrieu-Brunsen, A. J. S., Influence of chain architecture on nanopore accessibility in polyelectrolyte block-co-oligomer functionalized mesopores. *J Small* **2019**, *15* (41), 1902710.
37. Pardehkhorrani, R.; Andrieu-Brunsen, A. J. C. C., Pushing the limits of nanopore transport performance by polymer functionalization. *J Chemical Communications* **2022**, *58* (34), 5188-5204.
38. Soler-Illia, G. J.; Azzaroni, O. J. C. S. R., Multifunctional hybrids by combining ordered mesoporous materials and macromolecular building blocks. *J Chemical Society Reviews* **2011**, *40* (2), 1107-1150.
39. Xiao, K.; Wen, L.; Jiang, L. J. S., Biomimetic solid-state nanochannels: from fundamental research to practical applications. *J Small* **2016**, *12* (21), 2810-2831.
40. Förster, C.; Lehn, R.; Andrieu-Brunsen, A. J. S., Automated Multi- and Block-Copolymer Writing in Mesoporous Films Using Visible-Light PET-RAFT and a Microscope. *J Small* **2023**, *19* (16), 2207762.
41. Yameen, B.; Ali, M.; Neumann, R.; Ensinger, W.; Knoll, W.; Azzaroni, O. J. N. I., Synthetic proton-gated ion channels via single solid-state nanochannels modified with responsive polymer brushes. *J Nano letters* **2009**, *9* (7), 2788-2793.
42. Huang, K.; Szleifer, I. J. J. o. t. A. C. S., Design of multifunctional nanogate in response to multiple external stimuli using amphiphilic diblock copolymer. *Journal of the American Chemical Society* **2017**, *139* (18), 6422-6430.
43. Williams, T. M.; Zhou, Z.; Singh, S. S.; Sibrian-Vazquez, M.; Jois, S. D.; Henriques Vicente, M. d. G. J. P.; photobiology, Targeting EGFR Overexpression at the Surface of Colorectal Cancer Cells by Exploiting Amidated BODIPY-Peptide Conjugates. *J Photochemistry* **2020**, *96* (3), 581-595.

44. Strasser, P.; Russo, M.; Stadler, P.; Breiteneder, P.; Redhammer, G.; Himmelsbach, M.; Brüggemann, O.; Monkowius, U.; Klán, P.; Teasdale, I. J. P. C., Green-light photocleavable meso-methyl BODIPY building blocks for macromolecular chemistry. *J Polymer Chemistry* **2021**, *12* (47), 6927-6936.
45. Spanier, J. E.; Herman, I. P. J. P. R. B., Use of hybrid phenomenological and statistical effective-medium theories of dielectric functions to model the infrared reflectance of porous SiC films. *J Physical Review B* **2000**, *61* (15), 10437.
46. Boissiere, C.; Grosso, D.; Lepoutre, S.; Nicole, L.; Bruneau, A. B.; Sanchez, C. J. L., Porosity and mechanical properties of mesoporous thin films assessed by environmental ellipsometric porosimetry. *J Langmuir* **2005**, *21* (26), 12362-12371.
47. Dunphy, D. R.; Sheth, P. H.; Garcia, F. L.; Brinker, C. J. J. C. o. M., Enlarged pore size in mesoporous silica films templated by pluronic F127: Use of poloxamer mixtures and increased template/SiO₂ ratios in materials synthesized by evaporation-induced self-assembly. *J Chemistry of Materials* **2015**, *27* (1), 75-84.
48. Xiao, L.; Li, C.; He, X.; Cheng, X. J. S. A. S., BODIPY-based fluorescent polymeric probes for selective detection of Fe³⁺ ions in aqueous solution. *J SN Applied Sciences* **2021**, *3* (5), 591.
49. Zhu, J.; Han, H.; Li, F.; Wang, X.; Yu, J.; Qin, X.; Wu, D. J. C. o. M., Peptide-functionalized amino acid-derived pseudoprotein-based hydrogel with hemorrhage control and antibacterial activity for wound healing. *J Chemistry of Materials* **2019**, *31* (12), 4436-4450.
50. Lunn, J. D.; Shantz, D. F., Peptide Brush—Ordered Mesoporous Silica Nanocomposite Materials. *Chemistry of Materials* **2009**, *21* (15), 3638-3648.
51. Ruiz, D. S.; Cristobal, P. A.; Laurenti, M.; Retama, J. R.; Lopez-Cabarcos, E. In *Polymer Diffusion in Microgels with Upper Critical Solution Temperature as Studied by Incoherent Neutron Scattering*, Journal of Physics: Conference Series, IOP Publishing: 2014; p 012012.
52. Ksenofontova, K. V.; Ksenofontov, A. A.; Khodov, I. A.; Rumyantsev, E. V. J. J. o. M. L., Novel BODIPY-conjugated amino acids: Synthesis and spectral properties. *Journal of Molecular Liquids* **2019**, *283*, 695-703.
53. Ksenofontova, K. V.; Kerner, A. A.; Ksenofontov, A. A.; Shagurin, A. Y.; Bocharov, P. S.; Lukanov, M. M.; Kayumov, A. R.; Zhuravleva, D. E.; Iskhakova, Z. I.; Molchanov, E. E. J. M., Amine-Reactive BODIPY Dye: Spectral Properties and Application for Protein Labeling. *J Molecules* **2022**, *27* (22), 7911.

